J. Fluid Mech. (2004), *vol.* 503, *pp.* 161–170.
DOI: 10.1017/S0022112004007906 Printed in the United Kingdom

Low-order modelling of laminar flow regimes past a confined square cylinder

By B. GALLETTI[1], C. H. BRUNEAU[2], L. ZANNETTI[1] AND A. IOLLO[1]

[1]Dipartimento di Ingegneria Aeronautica e Spaziale, Politecnico di Torino, 10129 Torino, Italy

[2]Département de Mathématiques Appliquées, Université Bordeaux 1, Bordeaux, France

(Received 12 November 2003 and in revised form 26 December 2003)

A proper orthogonal decomposition based model is considered for two-dimensional vortex shedding past a confined square cylinder. The aim is to study the validity of such a model for Reynolds numbers and blockage ratios that are different from those for which the model was derived. Using a calibration procedure it is shown that reliable results can be obtained in terms of short-term (one period) dynamics. Long-term dynamics are accurately captured with a variation of the Reynolds number, whereas the error becomes large when the blockage ratio changes. The controllability and observability of vortex shedding at a slightly supercritical Reynolds number is investigated relying on the accurate low-order models obtained.

1. Introduction

The laminar two-dimensional flow past a square cylinder inside a plane duct presents flow features that make it attractive for the investigation of low-order models. It is a reasonable compromise between complexity of the physical phenomena and computational affordability.

A von Kármán vortex street develops past the cylinder when the Reynolds number increases above a critical value. This value is a function of the blockage ratio, i.e. the ratio between the cylinder side and the channel height. The resulting flow is characterized by the interaction of the vortical wake and the walls. The critical Reynolds number, based on the mass inflow, varies in the literature between 50 and 90 (Okajima 1982; Sohankar, Norberg & Davidson 1998; Breuer *et al.* 2000). Davis, Moore & Purtell (1984) discovered that the non-dimensional shedding frequency (the Strouhal number) reaches a maximum and then decreases as the Reynolds number increases. This phenomenon is generally ascribed to the shift of the separation point from the trailing to the leading square corners (Davis *et al.* 1984; Suzuki & Inoue 1993; Breuer *et al.* 2000).

The subject of this paper is low-dimensional modelling of such flow regimes using proper orthogonal decomposition (POD) (Lumley 1967). The Navier–Stokes equations are projected onto a low-dimensional function space and the ordinary differential equations that are obtained are solved instead of the full high-dimensional problem.

The purpose of this work is to assess the possibility of modelling a moderately complex flow over a range of flow parameters. This issue is important because POD functions are derived from existing databases of an experimental or numerical nature. Therefore, it is crucial to verify and possibly to enlarge the validity range of these models beyond the parameter values for which they were derived. This matter has

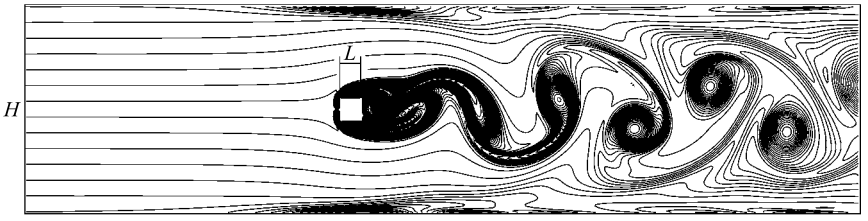

FIGURE 1. Definition of the geometry and a flow snapshot.

not yet been settled: Deane *et al.* (1991) tried an extrapolation of their POD models to different flow regimes. They considered a grooved channel flow and the flow past a circular cylinder. The results are contrasting: for the grooved channel flow the model extrapolates reasonably well over a range of Reynolds numbers, while for the cylinder case the extrapolation for different Reynolds numbers is very poor. Prabhu, Collis & Chang (2001) showed that various control laws affect the POD functions and also their energy ranking. Ma & Karniadakis (2002) instead found that by combining two sets of sub- and supercritical POD modes, it was possible to accurately reproduce the onset of three-dimensional instability in a circular cylinder wake.

An additional contribution of this work is the use of the linear control theory to elucidate the controllability and observability of a feedback controller based on the flow low-order model. Basic control tools are applied to our models with the assumption that since they provide a very accurate flow prediction, the control results can reasonably be extended to the full order problem. In particular we investigate the controllability and observability of vortex shedding past the cylinder at a slightly supercritical Reynolds number, using a linearized low-order model. This means that we could only control the linearly unstable modes, but these are the only unstable modes for slightly supercritical Reynolds numbers, see the discussion in Gillies (1998).

The flows considered in the next sections have a Reynolds number based on channel height which ranges from 60 to 255, and a blockage that ranges between 0.125 and 0.375. Due to confinement, within those limits the flow is believed to be still two-dimensional and laminar (Okajima 1982; Davis *et al.* 1984; Suzuki & Inoue 1993; Breuer *et al.* 2000).

2. Low-dimensional modelling

2.1. *Numerical simulation*

We deal with a flow around a square cylinder symmetrically placed between semi-infinite parallel walls (figure 1). The inlet velocity profile is parabolic. Channel length and cylinder position are optimized to minimize the influence of the inflow and outflow boundary conditions. Let L the length of the side of the square, H the height of the channel and $\beta = L/H$ the blockage ratio.

The flow field is obtained by numerical integration of the full non-dimensional Navier–Stokes equations (2.1). The simulation is achieved by means of a finite-difference multigrid method on a Cartesian mesh. The integration scheme is second order in space and time and reaches third-order accuracy for nonlinear terms. Special care is taken to ensure the non-reflectiveness of the exit artificial boundary. Details can be found in Bruneau & Fabrie (1994) and Bruneau (2000). The penalized

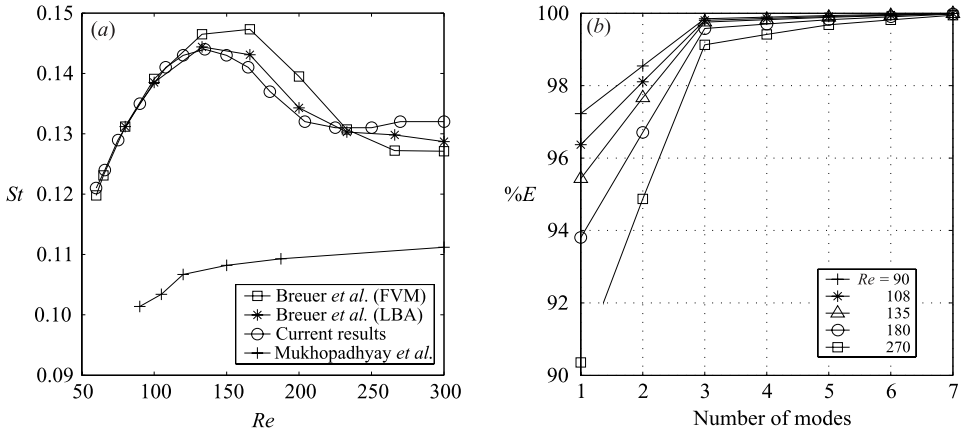

FIGURE 2. (*a*) Strouhal vs. Reynolds number ($\beta = 0.125$). FVM: finite volume method; LBA: lattice-Boltzmann method. (*b*) Represented energy vs. mode number for different Reynolds numbers ($\beta = 0.125$).

Navier–Stokes equations

$$\left.\begin{aligned} &\frac{\partial \boldsymbol{u}}{\partial t} + (\boldsymbol{u}\cdot\nabla)\boldsymbol{u} = -\nabla p + \frac{1}{Re}\Delta\boldsymbol{u} + \frac{\boldsymbol{u}}{K} \quad \text{in } \Omega \times (0, T), \\ &\nabla\cdot\boldsymbol{u} = 0 \quad \text{in } \Omega \times (0, T) \end{aligned}\right\} \tag{2.1}$$

are solved in the whole domain $\Omega = (0, 4H) \times (0, H)$ including the body up to time $t = T$. They are coupled to the no-slip boundary condition on the walls, Poiseuille flow at the entrance section and the artificial boundary condition mentioned above at the exit section, together with an initial datum at $t = 0$ on the velocity $u(., 0) = u_0$. The solid obstacle is considered as a medium of zero permeability ($K = K_s = 0$) while the fluid is considered as a medium of infinite permeability ($K = K_f = \infty$); numerically we set $K_s = 10^{-8}$ and $K_f = 10^{16}$. The grids are uniform and the resolution is the same both in the x- and y-directions with at least 32 points on the square side for the lowest blockage on the finest 1024×256 grid. Therefore, the number of points on the finest mesh is $M \simeq 250\,000$ for all of the investigated flows. The numerical results are validated by comparing the Strouhal–Reynolds curve we obtained to those in the literature (Breuer *et al.* 2000; Mukhopadhyay, Biswas & Sundararajan 1992), as shown in figure 2(*a*).

2.2. *POD–Galerkin model and calibration procedure*

Let us consider a data set that was obtained through a numerical simulation and arranged as N vectors $\{\boldsymbol{U}^{(1)}, \boldsymbol{U}^{(2)}, \ldots, \boldsymbol{U}^{(N)}\}$, where each vector represents a snapshot of the velocity field at a given time. The aim is to find a low-dimensional subspace of $\mathscr{L} = span\{\boldsymbol{U}^{(1)}, \boldsymbol{U}^{(2)}, \ldots, \boldsymbol{U}^{(N)}\}$ that gives the best approximation of $\mathscr{L}$. To this end we define a unit norm vector $\boldsymbol{\phi}$ that has the same structure as the snapshots and the largest mean square projection on the elements of $\mathscr{L}$. Following Sirovich's idea (Sirovich 1987) we express $\boldsymbol{\phi}$ as a linear combination of the snapshots, $\boldsymbol{\phi} = \sum_{n=1}^{N} b_n \boldsymbol{U}^{(n)}$, which leads to the eigenproblem $\boldsymbol{C}\boldsymbol{b} = \lambda\,\boldsymbol{b}$, where $C_{ij} = \boldsymbol{U}^{(i)^T}\boldsymbol{U}^{(j)}/N$ and $\boldsymbol{b} = [b_1, b_2, \ldots, b_N]^T$. The solution of the eigenproblem yields the eigenfunctions (POD modes) $\boldsymbol{\phi}_n$ that form a complete orthonormal set. The instantaneous velocity can be expanded in terms of the POD eigenfunctions: $\boldsymbol{u}(\boldsymbol{x}, t) = \sum_{n=1}^{N_r} a_n(t)\boldsymbol{\phi}_n(\boldsymbol{x})$. The original goal of obtaining a low-dimensional subspace which approximates the set $\mathscr{L}$ can be achieved by neglecting

the less energetic modes in the expansion, i.e. the modes that correspond to the smaller eigenvalues. In practice, since $\sum_{i=1}^{N_r} \lambda_i$ is proportional to the amount of energy contained in the first N_r modes, we choose N_r so that the ratio $\sum_{i=1}^{N_r} \lambda_i / \sum_{i=1}^{N} \lambda_i$ is for instance 99.99%. For our problem N ranges from 50 to 90, whereas N_r is around 20. We calculated the energy fraction contained in the first POD modes for a given blockage ratio and several values of the Reynolds number (figure 2*b*). Note that the number of POD modes that are necessary to represent a given energy level rises as the Reynolds number increases. Higher values of the Reynolds number correspond to more kinetic energy in the smaller scales, therefore more POD modes are necessary.

The POD modes integrate the obstacle and are divergence-free by construction. Hence, substituting the expansion of the velocity in terms of the POD modes into the weak formulation of Navier–Stokes equations and performing a Galerkin projection on the POD modes, one obtains the following nonlinear ordinary differential system:

$$\left.\begin{aligned} &\dot{a}_r(t) + B_{ksr} a_k(t) a_s(t) = -(\nabla p, \boldsymbol{\phi}_r) + \frac{1}{Re} D_{kr} a_k(t), \quad r = 1, \ldots, N_r, \\ &a_r(0) = (\boldsymbol{u}(\boldsymbol{x}, 0), \boldsymbol{\phi}_r), \quad r = 1, \ldots, N_r, \end{aligned}\right\} \tag{2.2}$$

where the Einstein notation for summations was used, (f, f) denotes the canonical l^2 inner product and the coefficients B_{ksr} and D_{kr} are real. The initial value problem (2.2) is a reduced-order model of the Navier–Stokes equations called the POD–Galerkin model. The projection term relevant to the pressure is a measure of the pressure drop along the channel: $-(\nabla p, \boldsymbol{\phi}_r) = \int_{\Gamma_i} p\, \boldsymbol{\phi}_r \cdot \boldsymbol{i}\, \mathrm{d}y - \int_{\Gamma_o} p\, \boldsymbol{\phi}_r \cdot \boldsymbol{i}\, \mathrm{d}y$ where Γ_i and Γ_o denote the inflow and the outflow section respectively and $\boldsymbol{i}$ denotes the unit vector in the x-direction. Unfortunately, the pressure cannot be easily expressed as a combination of POD modes. Therefore, we use a linear model of the relevant projection term, that is $-(\nabla p, \boldsymbol{\phi}_r) = C_{kr} a_k(t)$, where the real coefficients C_{kr} are computed as explained below. Hence system (2.2) yields

$$\left.\begin{aligned} &\dot{a}_r(t) = f_r(a_1, \ldots, a_{N_r}, C_{kr}) = -B_{ksr} a_k(t) a_s(t) + \left(C_{kr} + \frac{D_{kr}}{Re}\right) a_k(t), \\ &a_r(0) = (\boldsymbol{u}(\boldsymbol{x}, 0), \boldsymbol{\phi}_r). \end{aligned}\right\} \tag{2.3}$$

In view of the orthogonality of the POD modes, the inner product of the ith snapshot and the rth mode represents the reference value of coefficient $a_r(t)$ computed at the time t_i, that is, $a_r^{ex}(t_i) = (\boldsymbol{u}(\boldsymbol{x}, t_i), \boldsymbol{\phi}_r)$. Letting $\hat{a}_r(t)$ be the spline that interpolates the set of points $(t_1, a_r^{ex}(t_1)), \ldots, (t_N, a_r^{ex}(t_N))$, coefficients C_{kr} can be found by minimizing the functional $J' = \sum_{r=1}^{N_r} \sum_{i=1}^{N} (f_r(t_i) - \dot{\hat{a}}_r(t_i))^2$. The result of this least-square procedure is further refined by finding the extremum of $J'' = \sum_{r=1}^{N_r} \int_0^{t_N} (a_r(t) - \hat{a}_r(t))^2\, \mathrm{d}t$ under the constraints (2.3). The extremum of J'' is obtained by introducing a suitable Lagrangian function. The necessary conditions for the Lagrangian extremum define a direct-adjoint problem that converges quickly. These procedures can be viewed as a sort of calibration of the model on the given database and in principle can be extended to other applications.

For the case of $\beta = 0.125$ and $Re = 90$, in agreement with the results of Deane *et al.* (1991), the number of modes that are necessary to capture more than the 99.99% of the energy of the system is $N_r = 7$, as is seen in figure 2(*b*). Once the calibration matrix $\boldsymbol{C}$ is computed by means of the optimization procedure, the initial value problem (2.3) can be integrated in time. The results are the time histories of the mode amplitudes $a_r(t)$, which should be compared to those $\hat{a}_r(t)$ obtained by projecting the numerical data on the POD modes. The model predicts a stable limit cycle that exactly copies the one that corresponds to the full Navier–Stokes simulation for both small and

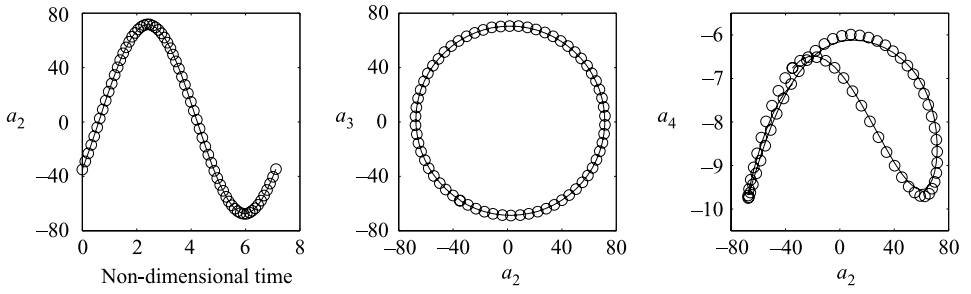

FIGURE 3. Prediction of the model for a Reynolds number not included in the database: comparison over the first shedding period between the mode amplitudes of model integration (solid lines) and numerical simulation (circles). $\beta = 0.125$ and $Re = 108$.

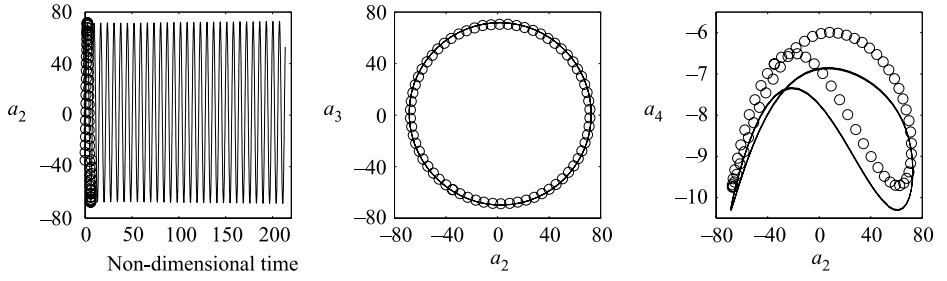

FIGURE 4. As figure 3 but after 30 shedding periods.

large time intervals. Thus the seven-equation POD–Galerkin model, with an even number of fluctuating modes and a mean flow mode, gives a precise description of both short- and long-term dynamics of the flow. Without calibration and keeping $a_1(t)$ constant (which basically gives the average flow), one obtains a limit cycle that shows a phase drift in time, but does not diverge.

2.3. *Model predictions as a function of the Reynolds number*

We applied the POD technique to extract an optimal basis from a mixed database that contains snapshots at different Reynolds numbers, see Ma & Karniadakis (2002), and at a fixed blockage ratio of 1/8. In particular we combined 51 snapshots at $Re = 90$, 55 snapshots at $Re = 135$ and 53 snapshots a $Re = 180$. We consider a model based on $N_r = 39$ POD modes extracted from these 159 snapshots. The snapshots belonging to the mixed database are reconstructed by the 39 POD modes with an error which is always less than 0.1% in terms of the snapshot kinetic energy. The 39-mode model is used to predict the flow behaviour for $Re \neq 90, 135, 180$. For instance, let us consider $Re = 108$, which locates a point in the increasing part of the St, Re curve (figure 2*a*). By calibrating the model on each of the three given sets of snapshots, one obtains three calibration matrices $\boldsymbol{C}_{90}, \boldsymbol{C}_{135}, \boldsymbol{C}_{180}$.

A quadratic interpolation can be performed: $\boldsymbol{C}(Re) = \boldsymbol{C}_{90}\,\psi_{90}(Re) + \boldsymbol{C}_{135}\,\psi_{135}(Re) + \boldsymbol{C}_{180}\,\psi_{180}(Re)$, where $\psi_{90}(Re)$, $\psi_{135}(Re)$, $\psi_{180}(Re)$ are the Lagrange interpolating polynomials based on the nodes $Re = 90, 135, 180$. This allows us to estimate the value $\boldsymbol{C}_{108} = \boldsymbol{C}$ (108) and then to solve the system of ODEs (2.3). The predictions of the model are then compared with the projection of a Navier–Stokes full simulation at $Re = 108$ on the current POD basis. The comparison is carried out over the first shedding period (figure 3) and after 30 shedding periods (figure 4): the predicted limit cycle is stable and converges on the full Navier–Stokes limit cycle for the second and

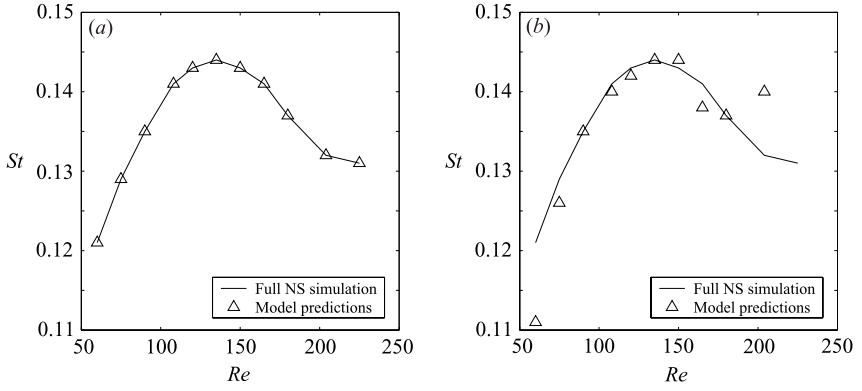

FIGURE 5. Strouhal–Reynolds curve computed by the low-order model: (*a*) over one shedding cycle; (*b*) over 30 shedding cycles. $\beta = 0.125$.

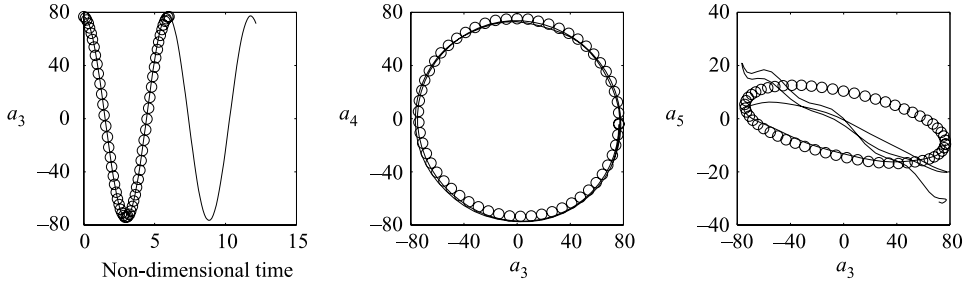

FIGURE 6. Prediction of the model for a blockage ratio not included in the database: comparison over two initial shedding periods between the mode amplitudes of model integration (solid lines) and numerical simulation (circles). $Re = 150$ and $\beta = 0.203$.

third modes. The model prediction of the Strouhal number at $Re = 108$ (not included in the database from which we extracted the POD modes) is obtained by taking the fast Fourier transform of the computed coefficient $a_2(t)$ over 30 shedding cycles. The result is a Strouhal value of 0.140 versus a full Navier–Stokes simulation value of 0.141, for a relative error of 0.7%.

It is interesting to repeat the preceding process for several values of the Reynolds number in the range 60 to 225 in order to construct the Strouhal–Reynolds curve predicted by the model. The curve obtained by integrating the model equation over a short time (figure 5*a*) exactly matches the one obtained by the full numerical simulation, whereas the analogous curve for a longer time integration (figure 5*b*) shows a loss of precision in the results.

2.4. *Model predictions as a function of the blockage ratio*

In this section we establish a low-order model that would be capable of capturing the essential features of the flow in the channel as the square size varies. A 31-equation model is calibrated on the numerical database relevant to $\beta = 0.125, 0.250, 0.375$ according to a procedure that is analogous to that described before.

By integrating the model for a value of the blockage ratio that is different from those used to build the POD basis one can observe that the long-term dynamics predicted by the model diverges. However the short-term prediction matches the full Navier–Stokes limit cycle for at least the third and fourth modes, as shown in figure 6

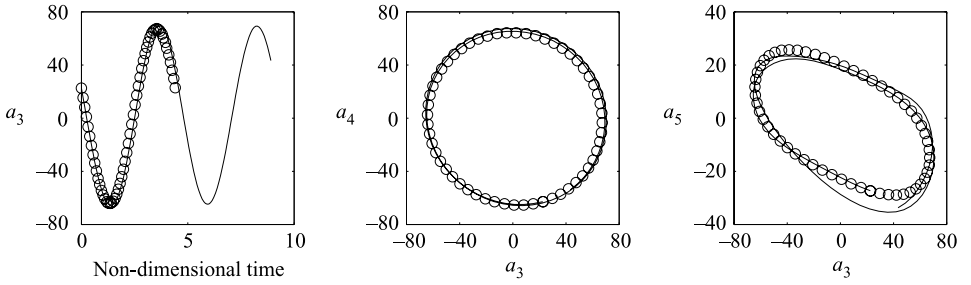

FIGURE 7. As figure 6 but for $\beta = 0.305$.

for $\beta = 0.203$ and in figure 7 for $\beta = 0.305$. The second POD mode is not oscillatory and has the same nature as the first one, in the sense that it is the correction of the mean flow caused by the variation of the blockage. The predictions of the POD–Galerkin model as a function of the blockage ratio are less accurate than those where the Reynolds number is varied. When the blockage ratio varies, the flow in the neighbourhood of the obstacle is affected. The mean flow is also considerably different because the two unsteady jets existing in the regions above and below the cylinder become increasingly intense with larger squares. Thus, for example, modes constructed for a blockage ratio of 0.125 and 0.250 cannot produce a precise solution for a blockage ratio of 0.203 in the cylinder neighbourhood, even if the calibration term accommodates the geometry and mean flow variation.

3. Flow controllability and observability

In this section we attempt an assessment of flow controllability and observability. An example is given where the model limit cycles are stabilized by feedback control.

The vortex street observed in the flow past a bluff body is due to a global flow instability (a global mode), which results from a region of local absolute instability in the near wake of the body (Huerre & Monkewitz 1990). As the Reynolds number is increased above the critical value Re_{cr} at which instability develops, other global modes appear besides the first one which is responsible for the onset of the vortex street. To control such flows, many global modes therefore have to be stabilized. Nevertheless, for a value of the Reynolds number that is slightly higher than Re_{cr}, it can be expected that the forcing required to control the flow is not large enough to destabilize the higher global modes. Hence, it seems reasonable to attempt the stabilization of the first unstable global mode by a linear feedback control strategy. For a blockage ratio of 0.125, to which a critical Reynolds number of 58 corresponds, we tried to stabilize the flow field at a Reynolds number of 66. The actuator action that was chosen is to vary the flow rate as it can be easily implemented in the low-order model.

We performed a numerical simulation of the flow that develops from the steady unstable solution at $Re = 66$. The steady unstable solution was obtained from the same code that was used for the unsteady simulations. The motion is impulsively started from rest. Initially a symmetric solution is formed with two attached recirculating regions, then the growing instabilities reach an amplitude which disrupts the base flow. After initialization from rest, the integration step was taken so small that we were able to identify the symmetric field with the minimal time residuals, of the order of 10^{-5} compared to 10^{-3} which is the usual time residual after the instability develops. This is taken as the steady unstable solution.

We extracted 67 snapshots during one period of the fully developed flow. Following the previously illustrated procedure, a $N_r = 7$ model was developed. Let $\overline{\boldsymbol{U}}$ denote the snapshot of the steady unstable solution. The equilibrium point that we want to stabilize is $\bar{a}_r = (\overline{\boldsymbol{U}}, \boldsymbol{\phi}_r)$. Expanding f_r as a power series about this equilibrium point and neglecting the second-order terms one obtains $\dot{a}_r(t) = f_r(\bar{a}_1, \ldots, \bar{a}_{N_r}) + J_{rj}(a_j(t) - \bar{a}_j)$ where $J_{rj} = -(B_{kjr} + B_{jkr})\bar{a}_k + C_{jr} + D_{jr}/Re$. By taking into account that $f_r(\bar{a}_1, \ldots, \bar{a}_{N_r}) \simeq 0$ the linearized state equation is $\dot{a}_r(t) = J_{rj}(a_j(t) - \bar{a}_j)$.

At the inlet section only the longitudinal component of the first mode is non-zero. The u velocity component is $u(0, y, t) = a_1(t)\boldsymbol{\phi}_1^u(0, y)$, and hence $a_1(t)$ provides a measure of the flow rate in the channel. This suggests the use of the following simple linear control law:

$$a_1(t) = \bar{a}_1 - \sum_{j=2}^{N_r} K_j(a_j(t) - \bar{a}_j). \tag{3.1}$$

Let us define the perturbation of the system from the equilibrium $\tilde{a}(t) = a(t) - \bar{a}$; then the linearized control system is

$$\dot{\tilde{a}}_r = A_{r-1,j-1}\,\tilde{a}_j + H_{r-1}u, \qquad r, j = 2, \ldots, N_r, \tag{3.2}$$

where $A_{r-1,j-1} = J_{rj}$, $H_{r-1} = J_{r1}$ and $u = -\sum_{j=2}^{N_r} K_j\,\tilde{a}_j$. A linear system is defined controllable if it can be led to any state from the zero initial state. A necessary and sufficient condition of controllability of the linear time-invariant system (3.2) on the interval $[0, T]$, for any $T > 0$, is $rank[\boldsymbol{H} \mid \boldsymbol{AH} \mid \boldsymbol{A}^2\boldsymbol{H} \mid \ldots \mid \boldsymbol{A}^{n-1}\boldsymbol{H}] = n$, where $n = N_r - 1$ is the size of matrix $\boldsymbol{A}$. In the present case the controllability matrix has a rank of 6 and hence system (3.2) is controllable.

Another major property of the system is the observability, that is the possibility of estimating the state from the output. As output we choose the wall stress measured along the channel walls between the abscissae x_1 and x_2. The relationship between the output $b(t)$ and the state $a(t)$ can be obtained by means of a least-square procedure that minimizes the functional $\int_{x_1}^{x_2}[\tau(x, 0, t) - \tau'(x, 0, t)]^2\,\mathrm{d}x + \int_{x_1}^{x_2}[\tau(x, H, t) - \tau'(x, H, t)]^2\,\mathrm{d}x$ where τ denotes the measured quantity and τ' is the wall stress in terms of POD modes. The solution is given by $b_k(t) = C_{kr}a_r(t)$ where

$$b_k(t) = \int_{x_1}^{x_2}\left[\frac{\partial u(x, 0, t)}{\partial y}\frac{\partial \boldsymbol{\phi}_k^u(x, 0)}{\partial y} + \frac{\partial u(x, H, t)}{\partial y}\frac{\partial \boldsymbol{\phi}_k^u(x, H)}{\partial y}\right]\mathrm{d}x, \qquad k = 1, \ldots, N_r,$$

$$C_{kr} = \int_{x_1}^{x_2}\left[\frac{\partial \boldsymbol{\phi}_k^u(x, 0)}{\partial y}\frac{\partial \boldsymbol{\phi}_r^u(x, 0)}{\partial y} + \frac{\partial \boldsymbol{\phi}_k^u(x, H)}{\partial y}\frac{\partial \boldsymbol{\phi}_r^u(x, H)}{\partial y}\right]\mathrm{d}x, \qquad k, r = 1, \ldots, N_r.$$

The problem that soon rises is that of determining the abscissae x_1 and x_2 in such a way that $C_{rj}^{-1}b_j(t)$ gives the best approximation of $\hat{a}_r(t)$ and $|x_1 - x_2|$ is as small as possible. We did not deal with this problem in a systematic way; however after some tests we have found that a reasonable compromise is given by measure segments placed $4L$ downstream to the cylinder centre and $3L$ long. This choice yields an error of reconstruction of the state variables $(1/N_r)\sum_{r=1}^{N_r}\sqrt{\int_0^{t_N}[C_{rj}^{-1}b_j(t) - \hat{a}_r(t)]^2\,\mathrm{d}t / \int_0^{t_N}\hat{a}_r(t)^2\,\mathrm{d}t}$ that is less than 1%.

The corresponding 7×49 observability matrix $[\boldsymbol{C}^T \mid \boldsymbol{J}^T\boldsymbol{C}^T \mid \ldots \mid (\boldsymbol{J}^T)^{N_r-1}\boldsymbol{C}^T]$ has a rank of 7: the linear system $\dot{\tilde{a}}_r = J_{rj}\tilde{a}_j$ is completely observable.

As an example, we stabilize the 7-equation model about the equilibrium point. We resort to a linear quadratic (LQ) regulator that finds the set of coefficients K_j that minimize the functional $\int_0^\infty(\tilde{a}_i\,\tilde{a}_i + u^2)\,\mathrm{d}t$ under the constraint of system (3.2). Once

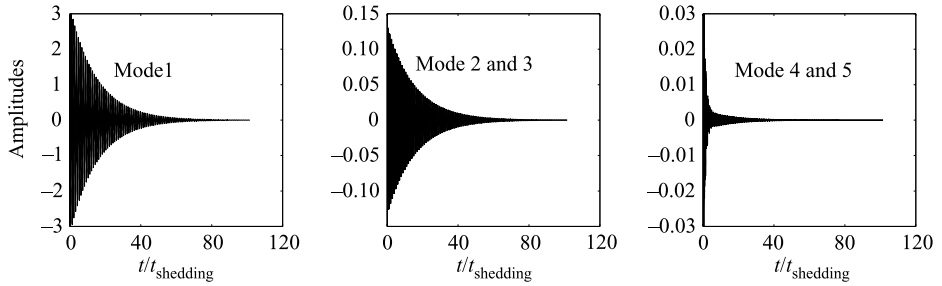

FIGURE 8. Time histories of the differences $\tilde{a}(t)$ between the mode amplitudes for the nonlinear controlled system and their corresponding equilibrium values. $\bar{a}_1 = 373$, $Re = 66$ and $\beta = 0.125$.

we have calculated the coefficients K_j by solving the associated Riccati equation, we integrate the original nonlinear system (2.3) with the control (3.1), starting from an initial state close to the equilibrium.

The results, in the form of perturbation $\tilde{a}(t)$, are depicted in figure 8. It is shown that a variation of the flow rate of less than 1% is sufficient to control the instabilities of the transient regime described by our low-order model.

4. Conclusions

A low-dimensional model of the flow past a square cylinder mounted inside a channel has been developed. The model was obtained from a Galerkin projection of the Navier–Stokes equations on the empirical eigenfunctions extracted from a database of a full numerical simulation by means of POD. We used this POD–Galerkin model to describe the flow for values of Reynolds numbers and of blockage ratio that were different from those used to extract the POD basis. The model is effective in capturing the short- and long-term dynamics for appreciable variations of the Reynolds number. The Strouhal–Reynolds curve, built on the basis of the short-term predictions of the model, accurately matches the one obtained by numerical simulation, a result that could be important for practical applications, e.g. in flow control. The model predictions as a function of the blockage are less accurate than those where the Reynolds number is varied. Nevertheless, it is possible to develop a low-order model that provides a fairly good representation of the short-term dynamics of the flow when the geometry is varied. We also considered the application of this POD–Galerkin modelling to study basic issues pertinent to the control of the wake past the cylinder. A 7-equation model of the transient regime was generated from a numerical database at $Re = 66$. The model was linearized about a state corresponding to the steady unstable solution of the Navier–Stokes equations at $Re = 66$, then its controllability and observability properties were proved. In particular, the state can be precisely estimated from stress measurements along a limited portion of the walls. The feedback control law deduced from the linearized system was given as input to the nonlinear system. It yielded the suppression of the instabilities of the transient regime with a variation of the flow rate of less than 1%. This wake model is very precise in capturing the limit cycle at $Re = 66$, therefore our conjecture is that at least controllability and observability will carry on to the full order model, i.e. the Navier–Stokes equations. The effectiveness of the linear control obtained on a problem governed by the full Navier–Stokes equations as well as the limits of validity of the linearized approach is the object of current investigations.

REFERENCES

Breuer, M., Bernsdorf, J., Zeiser, T. & Durst, F. 2000 Accurate computations of the laminar flow past a square cylinder based on two different methods: lattice-Boltzmann and finite-volume. *Intl J. Heat Fluid Flow* **21**, 186–196.

Bruneau, C. H. 2000 Boundary conditions on artificial frontiers for incompressible and compressible Navier-Stokes equations. *ESAIM Math. Mod. Num.* **34**, 303–314.

Bruneau, C. H. & Fabrie, P. 1994 Effective downstream boundary conditions for incompressible Navier-Stokes equations. *Intl J. Numer. Meth. Fluids* **19**, 693–705.

Davis, R. W., Moore, E. F. & Purtell, L. P. 1984 Numerical-experimental study of confined flow around rectangular cylinders. *Phys. Fluids* **27**, 46–59.

Deane, A. E., Kevrekidis, I. G., Karniadakis, G. E. & Orszag, S. A. 1991 Low-dimensional models for complex geometry flows: Application to grooved channels and circular cylinders. *Phys. Fluids* A **3**, 2337–2354.

Gillies, E. A. 1998 Low-dimensional control of the circular cylinder wake. *J. Fluid Mech.* **371**, 157–178.

Huerre, P. & Monkewitz, P. A. 1990 Local and global instabilities in spatially developing flows. *Anu. Rev. Fluid Mech.* **22**, 473–537.

Lumley, J. L. 1967 The structure of inhomogeneous turbulent flows. In *Atmospheric Turbulence and Radio Wave Propagation* (ed. A. M. Yaglom & V. L. Tatarski), pp. 166–178. Moscow.

Ma, X. & Karniadakis, G. E. 2002 A low-dimensional model for simulating three-dimensional cylinder flow. *J. Fluid Mech.* **458**, 181–190.

Mukhopadhyay, A., Biswas, G. & Sundararajan, T. 1992 Numerical investigation of confined wakes behind a square cylinder in a channel. *Intl J. Numer. Meth. Fluids* **14**, 1473–1484.

Okajima, A. 1982 Strouhal numbers of rectangular cylinders. *J. Fluid Mech.* **123**, 379–398.

Prabhu, R. D., Collis, S. S. & Chang, Y. 2001 The influence of control on proper orthogonal decomposition of wall-bounded flows. *Phys. Fluids* **13**, 520–537.

Sirovich, L. 1987 Turbulence and the dynamics of coherent structures, parts i, ii and iii. *Q. Appl. Maths* **XLV**, 561–590.

Sohankar, A., Norberg, C. & Davidson, L. 1998 Low-Reynolds number flow around a square cylinder at incidence: study of blockage, onset of vortex shedding and outlet boundary condition. *Intl J. Numer. Meth. Fluids* **26**, 39–56.

Suzuki, H. & Inoue, Y. 1993 Unsteady flow in a channel obstructed by a square rod (crisscross motion of vortex). *Intl J. Heat Fluid Flow* **14**, 2–9.